 doi:10.20944/preprints202204.0086.v1

Article

A Comprehensive Approach for Floodplain Mapping Through Identification of Hazard Using Publicly Available Data Sets Over Canada

Mohit Prakash Mohanty[1,2,*], and Slobodan P. Simonovic[2,*]

[1] Department of Water Resources Development and Management, Indian Institute of Technology Roorkee, Roorkee, 247 667, India
[2] Department of Civil and Environmental Engineering, Western University, London, Ontario N6A3K7, Canada
* Correspondence: mohit.mohanty@wr.iitr.ac.in

Abstract: Flood events and their associated damages have escalated significantly in the last few decades. To add to the gruesome situation, many reports and studies warn that flood risk would aggravate significantly in future periods due to significant alterations in the climate patterns and socio-economic dynamics. Floodplain mapping is looked upon as a viable option to tackle this global issue as it provides both quantitative and qualitative information on flood dynamics. Moreover, with the increasing availability of global data and enhancement in computational simulations, it has become easier to simlate flooding patterns at large scales. This study determines the usability of publicly available datasets in capturing flood hazards over Canada. Runoff data set from the North American Regional Reanalysis (NARR), along with a few other relevant inputs are fed to CaMa-Flood, a robust global hydrodynamic model to generate flooding patterns for 1 in 100 and 1 in 200-yr return period events over Canada . The simulated maps are compared and validated with the existing maps of a few flood-prone regions in Canada, thereby establishing their performance over both regional and country-scale. Later, the simulated floodplain maps are used in conjunction with property related information at 34 cities (within the top 100 populous cities in Canada) to determine the degree of exposure due to flooding in 1991, 2001, and 2011. The results indicate that around 80 percent of inundated spots belong to high and very-high hazard classes in a 200-yr event, which is roughly 4 percent more than simulated for 100-yr event. NARR derived floodplain maps perform very well while compared over the six flood-prone regions. While analyzing the exposure of properties to flooding, we notice an increase in the number during the last three decades, with the maximum rise observed in Toronto, followed by Montreal, and Edmonton. To disseminate the extensive flood-related information, a web-based public tool, Flood Map Viewer (http://www.flood-mapviewer.com/) is developed. The development of the tool was motivated by the commitment of the Canadian government to provide $63 M over the next three years for the completion of flood maps for higher-risk areas. The study reaches out to demonstrate how publicly available datasets can be utilized with a lesser degree of uncertainty in representing flooding patterns over large regions. The flood related information derived from the study can be used along with vulnerability for quantifying flood risk, which will help in developing appropriate pathways for resilience building for long-term sustainable benefits.

Keywords: Flood hazard; CaMa-Flood; Flood Map Viewer; Floodplain mapping; Flood risk; North American Regional Reanalysis; Property exposure

1. Introduction

In the last few decades, flood events have increased manifold leading to widespread human, environmental and economic losses (Winsemius et al., 2016; Kinoshita et al., 2018; Menéndez et al., 2020). Between 1980 and 2018, there were around 5,997 extreme flood events that resulted to approximately 223,482 fatalities, and a mammoth economic loss exceeding $1 trillion (Munich Re, 2018). In a recent report by UNISDR (2015), it is stated

 doi:10.20944/preprints202204.0086.v1

that flood-prone areas around the world houses around 800 million residents, of which about nearly one-tenth are exposed to floods on an annual basis. Apart from that, numerous scirntific researches signify that the disaster looming situation is expected to become more severe in the future periods due to alterations in climatic patterns and socio-economic dynamics (Wilner et al., 2018; Wing et al., 2018; Vousdoukas et al., 2018; Smith et al., 2019). In a recent study, Dottori et al. (2018) reported that with a rise in temperature up to 1.5 °C, human losses due to flooding at the global scale could rise to as high as 70–83%, including direct flood damages up to 160–240%. Under such circumstances, there is a dire need to both map and quantify the flood losses, to ensure optimum protection of the communities and assets.

Floodplain mapping provides qualitative (degree/severity of flood hazard) and quantitative (inundation extent, duration of flooding, inundation depth, etc.) information on flooding and is considered a viable option for minimizing flood risk. Most of the research on floodplain mapping has been demonstrated at small scales, i.e. local and regional. Considering the widespread damages, there was a growing need to extend it to larger scales at country, region and global levels. However, there were two significant challenges- (i) substantial computational efforts and, (ii) public availability of data sets. During the last decade, a significant progress has been made in tackling these two issues. In the recent times, a suite of global flood inundation models have been introduced by the scientific research community (Bernhofen et al., 2018; Boulange et al., 2021). These sophisticated tools are designed to quantify the flood inundation dynamics by using state-of-the-art algorithms. The flood hazard information is derived from the inundation parameters through suitable approaches (Winsemius et al., 2016; Alfieri et al., 2017; Mohanty et al., 2020). A list of the widely used global flood models is presented in Table 1. Recently, Gaur et al. (2018, 2019) employed CaMa-Flood to determine the timing of floods, and changes in their magnitudes across Canada during 2016-2100. In another research, Lim et al. (2018) utilized runoff observations of 11 GCMs belonging to the CMIP5 consortium as inputs to the CaMaFlood model to generate global river water depths. Earlier, Winsemius et al. (2013) developed a detailed framework in the GLOFRIS model, to determine flood hazards while utilizing climate-related datasets. The flood hazard estimates were later downscaled to higher resolutions of 1 km × 1 km by Ward et al. (2013) to account for the risk assessment.

Table 1. A list of widely used global flood models

Name of the model	Source
CaMa-Flood; Catchment-Based Macro-scale Floodplain model	http://hydro.iis.u-tokyo.ac.jp/~yamadai/cama-flood/
CIMA-UNEP; Centro Internazionale in Monitoraggio Ambientale and United Nations Environment Program model	https://www.preventionweb.net/organizations/8635
GLOFRIS; Global Flood Risk (model	https://www.globalfloods.eu/
JRC; Joint Research Centre model	https://ec.europa.eu/knowledge4policy/organisation/jrc-joint-research-centre_en
Fathom Global model	https://www.fathom.global/
LIS-FLOOD	http://www.bristol.ac.uk/geography/research/hydrology/models/lisflood/

On the other side, ready availability of public data sets such as Shuttle Radar Topography Mission (SRTM) DEM, MERIT DEM (Yamazaki et al., 2017); hydrologic and meteorological data from reanalysis products (Tarek et al., 2020; Wang et al., 2020), GCMs (Bermúdez et al., 2020; Toosi et al., 2020); and tide data from global tide elevation (Hunter et al., 2017), have made it easier to develop comprehensive flood model set-ups to derive hazard values. The reanalysis datasets are generated by weather forecasting models in the

 doi:10.20944/preprints202204.0086.v1

form of two-dimensional gridded data sets (Compo et al., 2011). They serve as an alternative for those regions, where station-level observations are scant or sparsely available. Only a few studies have readily utilized the reanalysis datasets to reproduce flood inundation dynamics, most of them focusing on regional scales. Gründemann et al. (2018) used the global Water Resources Reanalysis (WRR) dataset for characterizing floods over the Limpopo River basin in Southern Africa. The authors found that the models are competent in capturing flood events over stations with a large upstream catchment area. To explore the efficacy of reanalyses products in reconstructing hydro-meteorological hazardous events at the regional scale, Senatore et al. (2020) performed dynamical downscaling of two global reanalyses- ERA-Interim and ERA5 and used them in WRF-Hydro modeling system.

Among all the known natural disasters in Canada, floods are known to be the most severe ones, as they constitute the largest costs for recovery (NRCan, 2018). During 1970 and 2015, the total number of flood events has increased significantly (Public Safety Canada, 2017). Therefore, identifying and quantifying flood risks is a major requirement to develop robust adaptation measures and resilience mechanisms. Being the second largest country in the world, research and development on various domains of flood management are carried out at the level of each province. Because of this, there is absence of a unified methodology that is nationally accepted. Under these situations, it is crucial that a nationwide floodplain mapping be carried out to disseminate the information to the end-users. Recently, a Federal Floodplain Mapping Guidelines Series was launched by the Public Safety Canada that covers all components of the flood mitigation process. The extensive framework consists of four main blocks, namely (i) Flood Hazard Identification and Priority Setting, (ii) Hydrologic and Hydraulic Procedures for Flood Hazard Delineation, (iii) Geomatics Guidelines for Floodplain mapping, and, (iv) Risk-based Land-use Guide.

Based on the extensive literature review, it is now well established that quantifying flood inundation dynamics over large scales has become easier than before with the increasing availability of public datasets, and global flood models. The present study evokes the usability of publicly available datasets for carrying our floodplain mapping and deriving flood hazards over Canada. The next section provides details on various datasets and flood model used to simulate flooding patterns for various scenarios. This section also elaborates on the derivation of flood hazard from inundation values. It is followed by details on the quantification of property exposure due to concurrent flooding over the last three decades. The last portion describes the development of a web-based flood information tool. Section 3 provides the results and discussions on inundation mapping, hazard modeling, validation of floodplain maps, and degree of property exposure. The last section gathers the conclusions on the study.

2. Materials and Methods

The proposed framework for capturing flood hazards through floodplain mapping is illustrated in Figure 1. The comprehensive framework is comprised of two major blocks, namely, (i) selection of runoff observations (as input data set), and (ii) CaMa-Flood model (for simulating floodplain mapping). The individual blocks are described in detail in the following sections.

2.1 North American Regional Reanalysis (NARR)

In this study, we utilize the readily available NARR reanalysis product, which is a high-resolution dataset containing various atmospheric and land surface hydrology variables for the North American region (Mesinger et al., 2006). The observations embedded in NARR were derived while making improvements on NCEP-NCAR reanalysis datasets (Ashtine et al., 2016). The runoff data from 1979 to present day is available at a temporal resolution of every three hours, and surface resolution of 0.3° × 0.3°.

2.2 Catchment-based Macro-scale Floodplain (CaMA-Flood) Model

Preprints (www.preprints.org) | NOT PEER-REVIEWED | Posted: 11 April 2022 doi:10.20944/preprints202204.0086.v1

The CaMa-Flood model is one of the well-known tools that has been used widely to simulate the hydrodynamics of flood waves, especially over large regions (Mohanty et al., 2021). The CaMa-Flood considers the discretized version of river networks in the form of hydrological units, othwerwise referred to as unit-catchments. The water storage within each unit-catchment decides the water levels and inundation extent. This is ensured by considering the sub-grid topographic parameters of overland bathymetry and channel. For the river network map, CaMa-Flood utilizes a grid-based hybrid river network. Such an arrangement connects one grid to the adjoining unit-catchment, resulting to a realistic parameterization of the sub-grid topography. The local intertial equation calculates the channel discharge and velocity (Bates et al., 2010). On the other hand, water storage is decided by the water-balance equation.

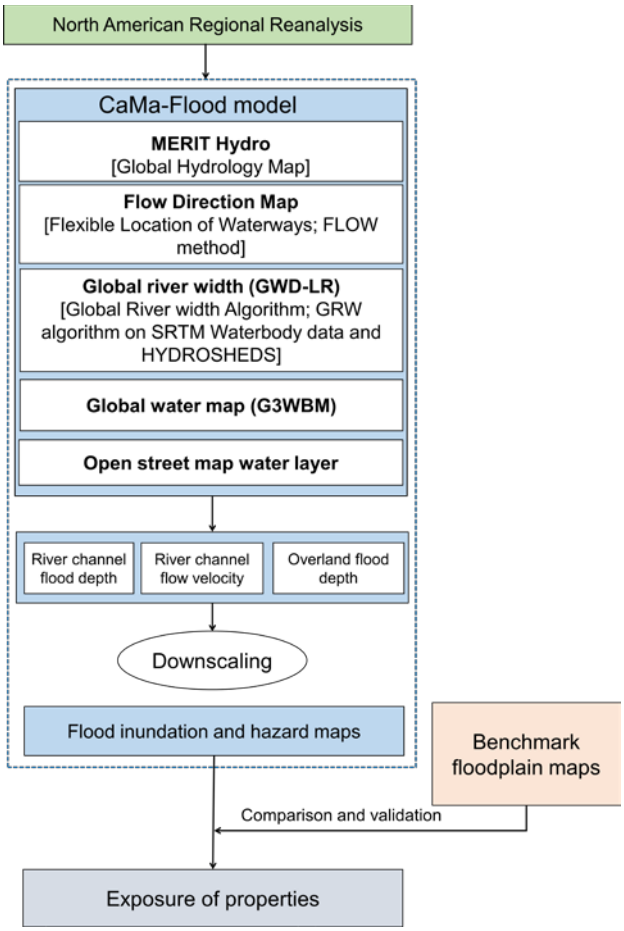

Figure 1. A proposed framework of floodplain mapping

One of the major advantages of CaMa-Flood is the explicit representation of flood-related outputs (water level and flooded area). Being a 2D model, the results derived from CaMa-Flood can be compared and validated both at the 1D i.e. river channel and 2D i.e. overland inundation level. Compared to the other existing models, CaMa-Flood provides high numerical efficiency for simulating inundation dynamics for large regions. The overland inundation is determined through a robust diagnostic scheme at the unit-catchment scale. The local intertial equation, along with the adaptive time step scheme optimize the computation of channel discharge and water storage (Bates et al., 2010; Hunter et al., 2005).

2.2.1 Components of the CaMa-Flood model

Preprints (www.preprints.org) | NOT PEER-REVIEWED | Posted: 11 April 2022 doi:10.20944/preprints202204.0086.v1

Flow Direction Map- An upscaling algorithm, namely, The Flexible Location of Waterways (FLOW) method as introduced by Yamazaki et al., (2009) is used to create a relatively low-resolution river network map from a higher resolution. This method is also utilized to generate sub-grid-scale topographic parameters of the coarse river network such as length of the channel and its level, elevation of the floodplain, and unit-catchment area.

Global River Width (GWD-LR)- Yamazaki et al., (2014) presented a robust algorithm to derive the Global Width Database for Large Rivers (GWD-LR), while implementing it over the SRTM water body mask and flow direction map. In this data, the river-widths from bank to bank and effective level are provided. It has been observed that the effective river width in this dataset is comparively narrower when compared against a few other exisiting sources, however, relative difference not exceeding 20%. Moreover, as the river widths are derived from a reliable flow direction map, application of GWD-LR for large-scale modeling is expected to contain less error percentages.

Global Water Map- The Water Body Map (G3WBM) was introduced by Yamazaki et al. (2015). The authors developed an automated algorithm that holds the capacility to process numerous Landsat images from the Global Land Survey (GLS) database at various temporal scales. To create a noise-free map of water body map, they considered around 33,890 scenes from 4 GLS epochs. The water map is also free from ice/snow gaps, and cloud covers. To distinguish the permanent water-bodies from the temporary ones, the-frequency of water body was identified by overlapping multi-temporal Landsat images. It has also been observed that the G3WBM efficienctly separates river channels and adjoining floodplains more precisely than other competitive datasets.

OSM Water Layer- Yamazaki et al. (2019) introduced OSM Water Layer, which is a global surface water data. The extensive information is derived by extracting water masks from the OSM. The OSM Water Layer is available freely in both PBF and GeoTiff formats. The raster version of the map has four categories, i.e. Major river, large rivers and lakes, minor streams, and canal.

2.3 Methodology of floodplain mapping

Firstly, NARR runoff datasets are aggregated to a daily time scale. The runoff estimates within each grid for 100 and 200-yr events are generated through extreme value analysis using Generalized Extreme Value (GEV) distribution. This distribution has an upper bound and a flexible tail. GEV is given by:

$$F(x)=\exp\left\{-\left[1-\frac{k(x-\mu)}{\sigma}\right]^{1/\xi}\right\},\ k\neq 0 \quad (1)$$

$$F(x)=\exp\left\{-\exp\left(-\frac{x-\mu}{\sigma}\right)\right\},\ k=0 \quad (2)$$

where μ, σ, and k are the location, scale and shape parameters, respectively.

The 100 and 200-yr runoff calculated at every grid is considered as an input to the CaMa-Flood to generate flood inundation parameters, namely inundation depth and extent. Later an efficient downscaling procedure is implemented over the coarse maps to generate high resolution maps at a resolution of 1 km. The floodplain maps for a few regions are extracted and compared with the existing regional maps of flood-prone regions.

2.4 Determination of flood hazard

The range of inundation depths derived through flood inundation modeling is utilized to derive flood hazard values from very-low to very-high. The discretization of hazard values is governed based on the degree of damages to physical assets and human beings (Mohanty et al., 2020). Assuming '(d_n)' is the depth of inundation associated with each p^{th} grid in the considered domain, the value of flood hazard $\boldsymbol{\check{H}}$ depends upon $d_n \in \mathbf{D}$ $\forall\ p \in \mathbf{P}$. Here $\mathbf{D}$ denotes the set of all flood depths. The flood hazard $\boldsymbol{\check{H}}$ may be expressed as f(D) as described below

Preprints (www.preprints.org) | NOT PEER-REVIEWED | Posted: 11 April 2022 doi:10.20944/preprints202204.0086.v1

ζ: $\mathbf{D} \rightarrow \check{\boldsymbol{H}} \in \mathbf{R}^{+}$ such that

$\delta = \zeta((d_1),\ldots,(d_n)); \delta \in \check{\boldsymbol{H}}; p \in \mathbf{P}$ and $(d_1), \ldots, (d_n) \in \mathbf{D}$ (**2**)

where $\mathbf{R}^{+}$ represents the set of positive real numbers, while 'p'denotes the total grid cells.

Based on the hazard estimates, the values of $\zeta((d_1),\ldots,(d_n))$ is discretized into five classes as dexcribed in Equations (3), and (4):

$\Omega_d: \check{\boldsymbol{H}} \rightarrow \check{H}_d; \check{H}_d = \{h_d \in \mathbf{P}: h_d \leq 5$ (**3**)

$$d_h = \begin{cases} 1, & 0 \leq d \leq 0.2 \\ 2, & 0.2 < d \leq 0.6 \\ 3, & 0.6 < d \leq 1.5 \\ 4, & 1.5 < d \leq 3.5 \\ 5, & d > 3.5 \end{cases} \quad (4)$$

where d and d_h represent the value of flood hazard and its index for the p^{th} grid.

2.4 Quantification of exposure of properties due to flooding

The simulated floodplain maps for Canada are further utilized to quantify the degree of exposure of properties. The property footprints for 1991, 2001 and 2011 is obtained from the housing statistics, Statistics Canada (www.statcan.gc.ca). Based on data availability, 34 cities are considered, which also fall in the list of 100 most populous cities in Canada (Gaur et al., 2019). The footprints of properties are overlaid on the floodplain maps simulated during the corresponding years to estimate the number of properties exposed due to concurrent flooding.

2.5 Development of Flood map viewer

To disseminate the flood related information to various stakeholders, as well as local communities in Canada, Flood Map Viewer (http://www.floodmapviewer.com/)-a web-based public tool, is developed. The web-based tool considers the entire Canada as the base-map and presents flood-related information for 100-yr and 200-yr of various historical and climate change scenarios at a high resolution of 1 km × 1 km. A special attention is given to user-friendliness to ensure that the information can be understood by a non-technical audience as well (Mohanty et al., 2021).

3. Results

3.1. Floodplain maps derived by utilising NARR

The 100-yr and 200-yr runoff are considered as inputs to the CaMa-Flood model to generate Canada-wide floodplain maps. These maps are illustrated in Figure 2 overlaid on the Digital Elevation Model. The percentage of maximum water depth, an indicator of flood hazard is illustrated in the form of pie-charts insaide these maps. We notice that about 10.10 percent of inundated regions fall within low hazard category (depth below 0.2 m) during 100-yr (Figure 2 a) as compared to 9.68 percent for a 200-yr flood event (Figure 2 b). On the contrary, the cumulative percentage classes is close to 80 percent for the latter, which is roughly 4 percent more as observed during the 100-yr event. The remaining classes of flood hazard for a 100-yr and 200-yr events constitute 8.72 and 7.89 percent (low hazard), 5.03 and 2.72 percent (medium hazard). The very-low and low flood hazard classes are mostly found over the northern and central parts of Canada. The efficacy of representing extreme events by NARR over Canada is well documented in the recent literature (Kim et al., 2008; Mohanty et al., 2021). The observations conform the good performance of NARR as a suitable input parameter, as it is able to capture the high-, and very-high hazard spots well. In a recent article, Essou et al. (2016) highlight that NARR uses a 3D-VAR assimilation approach that provides high efficiency in representing extreme events such as floods.

Preprints (www.preprints.org) | NOT PEER-REVIEWED | Posted: 11 April 2022 doi:10.20944/preprints202204.0086.v1

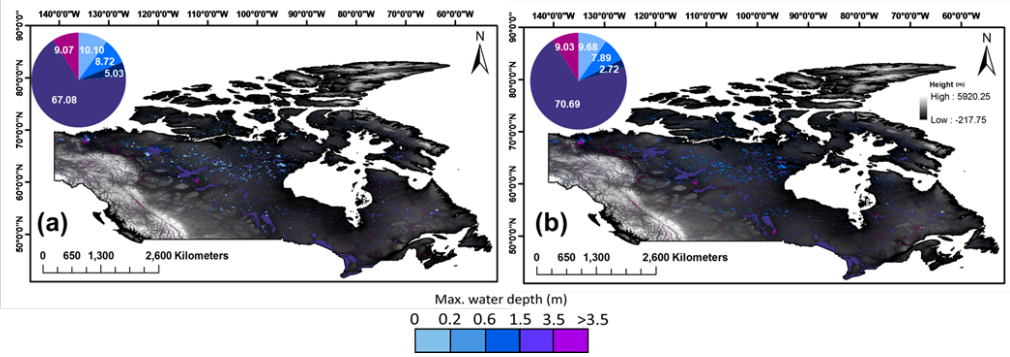

Figure 2. 100-yr and 200-yr floodplain maps derived by utilisng NARR. The inset pie-chart provides details on the percentage of area exposed to a particular degree of flood hazard

3.2. Validation of floodplain maps with benchmark maps

The 100-yr and 200-yr floodplain maps generated through computational modeling are compared with a few existing floodplain maps over six regions in Canada. The spatial flood related information in these maps is obtained from the respective basins by considering precise and extensive input data sets such as high resolution topography, river cross-section details etc., while using a regional flood inundation model. As such the comparison of simulated floodplain maps with the existing ones over the regions will ensure the performance of flood model. Figure 3 illustrates the comparison of simulated and existing floodplain maps over six regions, namely, Lower Fraser River Basin, Grand River basin, St. John Basin, Calgary basin, Assiniboine Basin, and Red River basin. Overall all the simulated maps perform well in representing the inundation dynamics over these regions. While comparing the flood inundation over Fraser Basin (geographical extent~11,134 km^2) for 100-yr and 200-yr, we notice that more than 3/4th of inundated spots in the existing floodplain maps comply with the simulated ones (Figure 3a). With 200-yr map, we notice underestimation of a few spots in the western coastal region as highlighted by red coloured grids. This is due to the fact that the flood model setup considered in this study accounts for the riverine inundation. While demonstrating the comparison over Calgary Basin (geographical extent~ 1345 km^2), we notice a high degree of similarity with the existing floodplain maps. Earlier, Sampson et al. (2015) also noticed a similar behavior while comparing their simulated floodplain maps over Calgary. The authors used SRTM DEM to represent the topographical features in the flood model. The present study exhibits a higher degree of similarity with the benchmark floodplain map, due to consideration of MERIT DEM, in which significant noise corrections over SRTM DEM has been conducted. Past researches have confirmed a high degree of performance of MERIT DEM in floodplain mapping, synonymous to LiDAR DEMs over various case-studies (Hawker et al., 2018; Liu et al., 2021; Hao et al., 2021; Kirezci et al., 2020). The Assiniboine Basin (geographical extent~1,62,000 km^2) is a large river basin consisting of Qu'Appelle, Souris, and Assiniboine sub-basins. Past flood events in 2011 and 2014 that took place in this region incurred huge economic and physical losses. Blais et al. (2016) regard the 2011 event as the most extreme event that Canada had witnessed. The NARR derived floodplain maps for both scenarios match the benchmark floodplain inundated spots. A slight discrepancy is noticed over the northern and eastern parts. The possible reason for this observation is the rapid changes in the channel slope of the Assiniboine river at various chainages over the study region, which may not be precisely captured by the MERIT DEM (Tavares da Costa et al., 2019). The red river basin (geographical extent~1,19,000 km^2) resides beside the Assiniboine basin. As the red river flows northwards, it follows a meandering river course, which aggravates the chances of inundation near the floodplains during extreme weather events. The flood event that occurred in 1997 over the Red river basin is often

Preprints (www.preprints.org) | NOT PEER-REVIEWED | Posted: 11 April 2022 doi:10.20944/preprints202204.0086.v1

referred to as the "Flood of the Century" (Rannie, 2016; Simonovic, 1999). Through a visual comparison, it is clear that the simulated floodplain matches very closely with the existing flood inundated spots. The complete riverine inundation is adequately simulated over the study extent. A limited number of small stream networks are left behind. This is due to the inclusion of Global River Width data as an input, which is not able to identify river widths of size lesser than 183 m. The Grand Basin (geographical extent~6,800 km²) in Southwest Ontario consists of three distinct landforms: plains in the northern and western parts, moraines in the eastern and central parts, and clay in the southern part. Rapid snowmelt, in tandem with concurrent rainfall and high surge are the major flood drivers in this region. The simulated floodplain maps capture the inundated spots competitively.

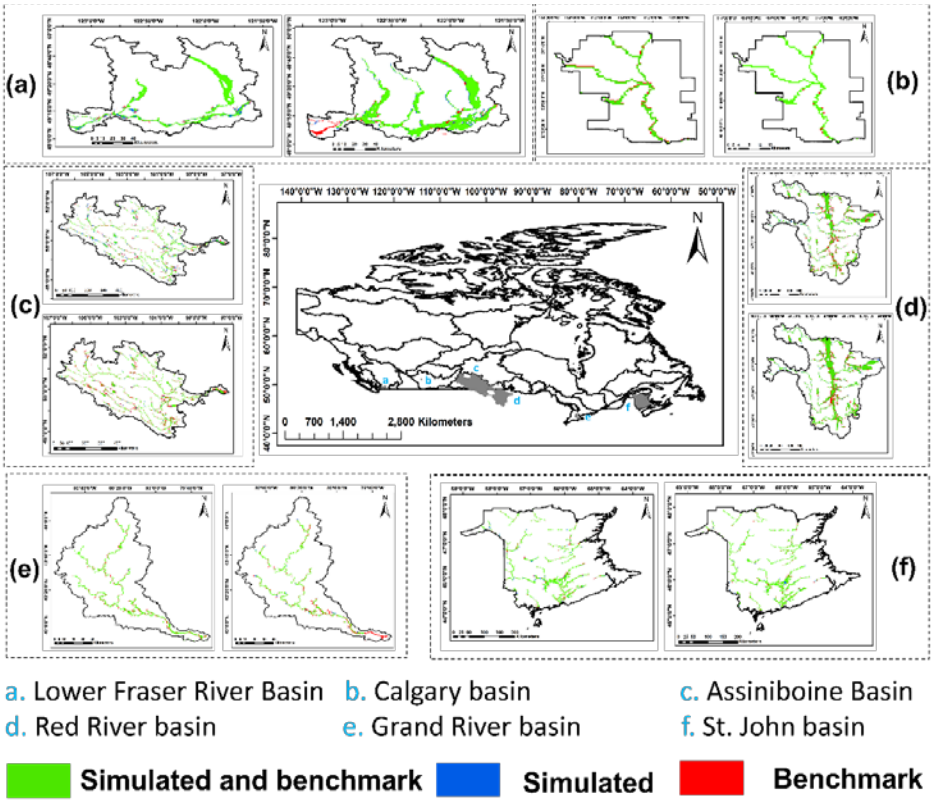

Figure 3. Comparison and validation of generated floodplain maps (both for 100-yr and 200-yr) against existing ones over six flood-prone regions of Canada

A slight underestimation is seen with 200-yr floodplain map, however, over the lower stretch of the basin. The St. John Basin (geographical extent ~12,222 km²) is situated between Quebec and New Brunswick. The major driver to concurrent flooding occurs during the months of April to May from the runoff resulting from melting snowpack. One of the major spring flooding was seen in 2008, when relatively warmer climate resulted in a higher melting of snowpack. Despite the fact St. John basin is a coastal region, the inundated spots over the southern stretches are simulated fairly well by NARR (Figure 3f). A few areas of over predicted and under predicted grids are noticed, which are possibly due to the presence of noise in MERIT DEM elevation values.

3.3 Exposure of property to flooding at a decadal time scale

The property footprints were overlaid on the floodplain maps simulated for 1991, 2001 and 2011 with NARR dataset. As mentioned in Section 2.4, a set of 34 cities falling in the category of 100 most populous cities of Canada were collected based on the data availability. The distribution of these cities over the provinces is as follows- two cities each

Preprints (www.preprints.org) | NOT PEER-REVIEWED | Posted: 11 April 2022 doi:10.20944/preprints202204.0086.v1

in Alberta, Saskatchewan, and New Brunswick; four cities in British Columbia; fifteen cities in Ontario; six cities in Quebec; one city each in Manitoba, Nova Scotia, and New Foundland and Labrador.

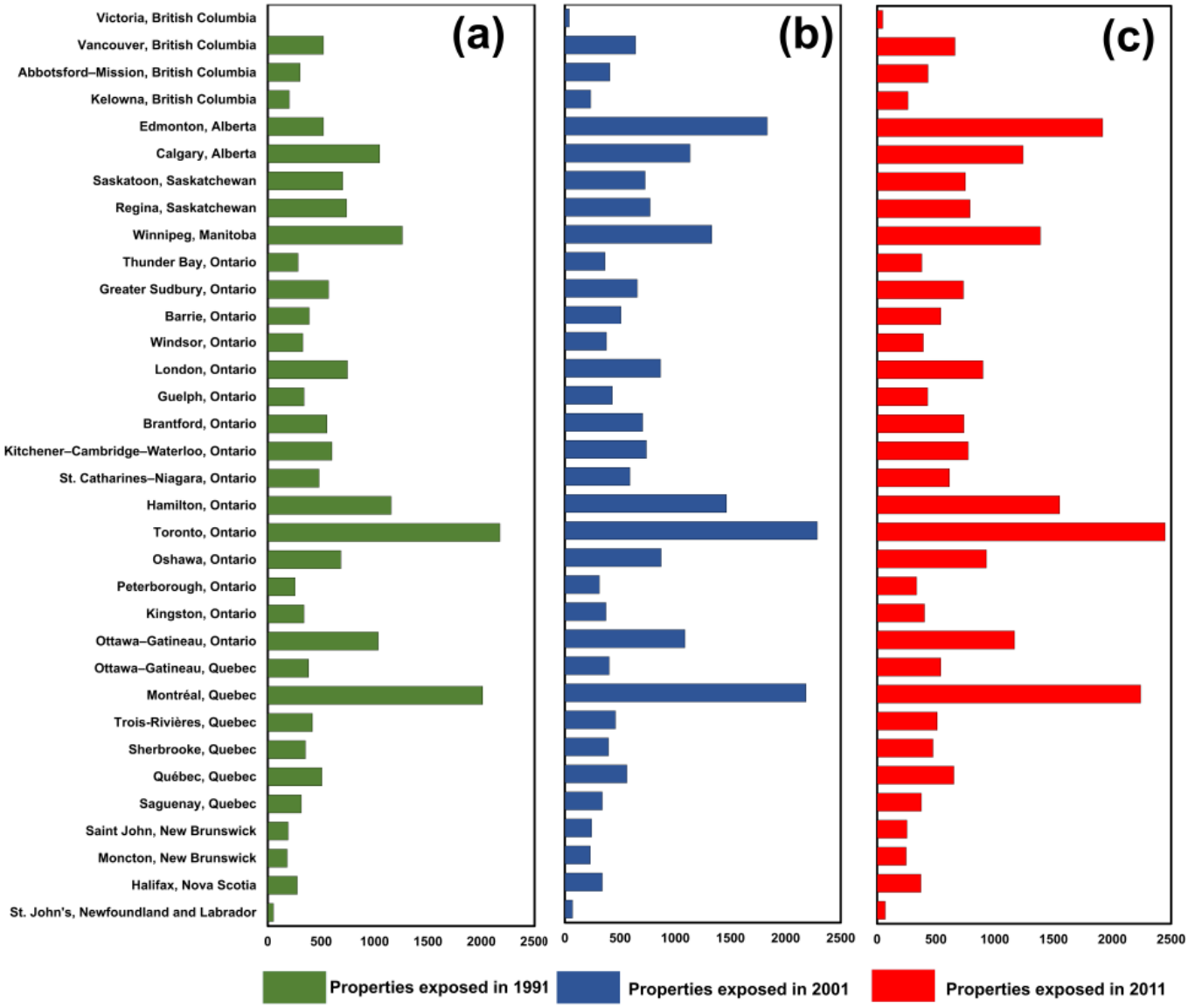

Figure 4. Number of properties exposed to flooding in 1991, 2001 and 2011

The number of property exposed to concurrent floods in 1991, 2001 and 2011 is illustrated in Figure 4. Overall, there is an increase in the number of properties exposed to flooding in the last three decades. Cities such as Vancover, Victoria, and Abbotsford-Mission in British Coumbia showed more or less an increase in the properties exposed to flooding in 2001 and 2011. Edmonton recoded a steep increase of nearly four times in the number of properties exposed to floods in 2011 as compared to 1991. Our results are supported by the recent fidings by Chakraborty et al. (2021), who reported that British Columbia contains the second highest percentage of population exposed to flooding. Most cities in Ontario depict a rise in the numbers, the maximum being in Toronto (1997 in 1991, 2020 in 2001, and 2455 in 2011), followed by Hamilton 1224 in 1991, 1522 in 2001, and 1601 in 2011). A similar pattern is noticed over Quebec, where the number of properties exposed to flooding remained high (more than 2,000) through out the decades. The remaining cities

 doi:10.20944/preprints202204.0086.v1

in Quebec did not show a rapid change in the numbers over the years.Cities in New Brunswick show a sparse number of properties exposed to flooding, in a similar way over Nova Scotia, and New Foundland and Labrador.

3.4 Flood map viewer

As highlighted in Section 2.5, Flood Map Viewer is a web-based tool that is developed to disseminate the Canada-wide flood-related information. The tool is aimed to help raise awareness of the general public, professionals in the field and responsible agencies to both, existing flood risk in Canada and its change under future climate conditions. The overlay of postal codes (available in the floodmapviewer) allows search for potential impacts up to the street and property level. Upon opening the website, the first page shows details on various options, namely, Maps, Download, Lean More, and User Guide (Figure 5). To explore the flood maps, user can click on the 'Maps' option. In the top of this page, various options for overlaying on the base map, such as Canada DEM, Drainage basins, Postal codes are present (Figure 6,a and b).

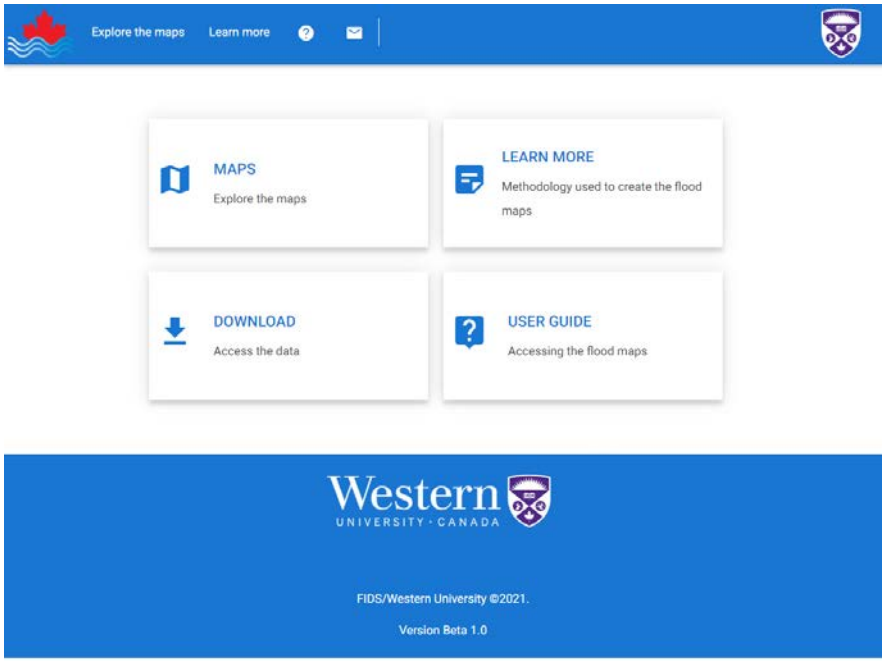

Figure 5. A screenshot of the first page of Flood Map Viewer

Preprints (www.preprints.org) | NOT PEER-REVIEWED | Posted: 11 April 2022 doi:10.20944/preprints202204.0086.v1

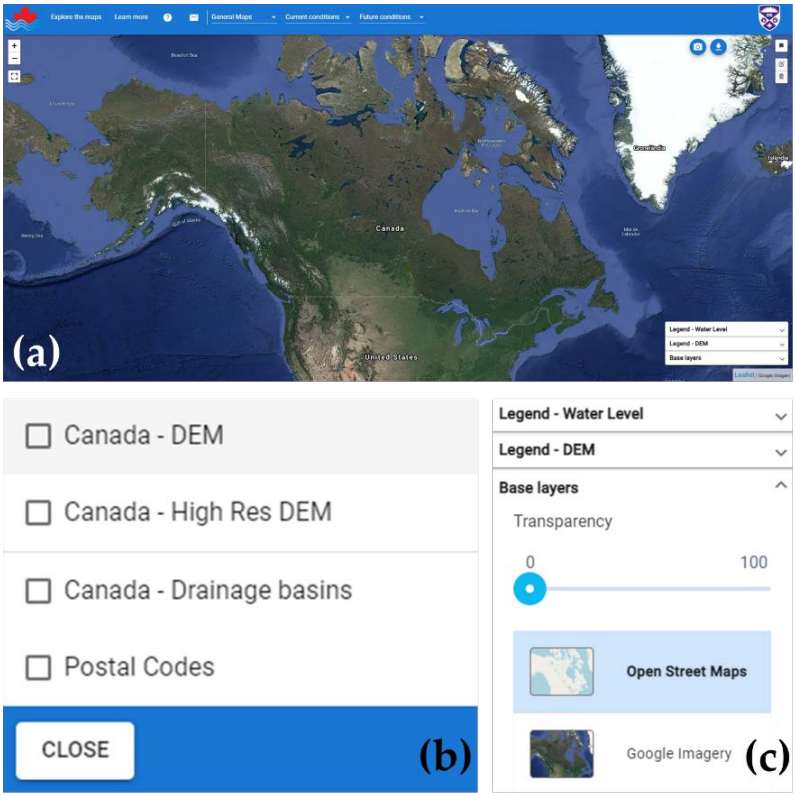

Figure 6. A screenshot of the "Maps" option in Flood Map Viewer

The second and third option provides details on the flood-related maps for the current and future conditions). Users have the flexibility to change the transparency, and change the base map to open streets map or google earth imagery as per their requirement (Figure 6,c). The flood-related maps are also available for download in the 'Download' option of the first page. After clicking on this option, a set of files ranging from flood maps to spatial boundaries are available for free download. The entire methodology used for floodplain mapping is described in the 'Learn More' option. The last option 'User Guide' provides a step-by-setp guide for accessing the flood-related information in the website for any user. A represntative flood plain map is illustrated in Figure 7.

Preprints (www.preprints.org) | NOT PEER-REVIEWED | Posted: 11 April 2022 doi:10.20944/preprints202204.0086.v1

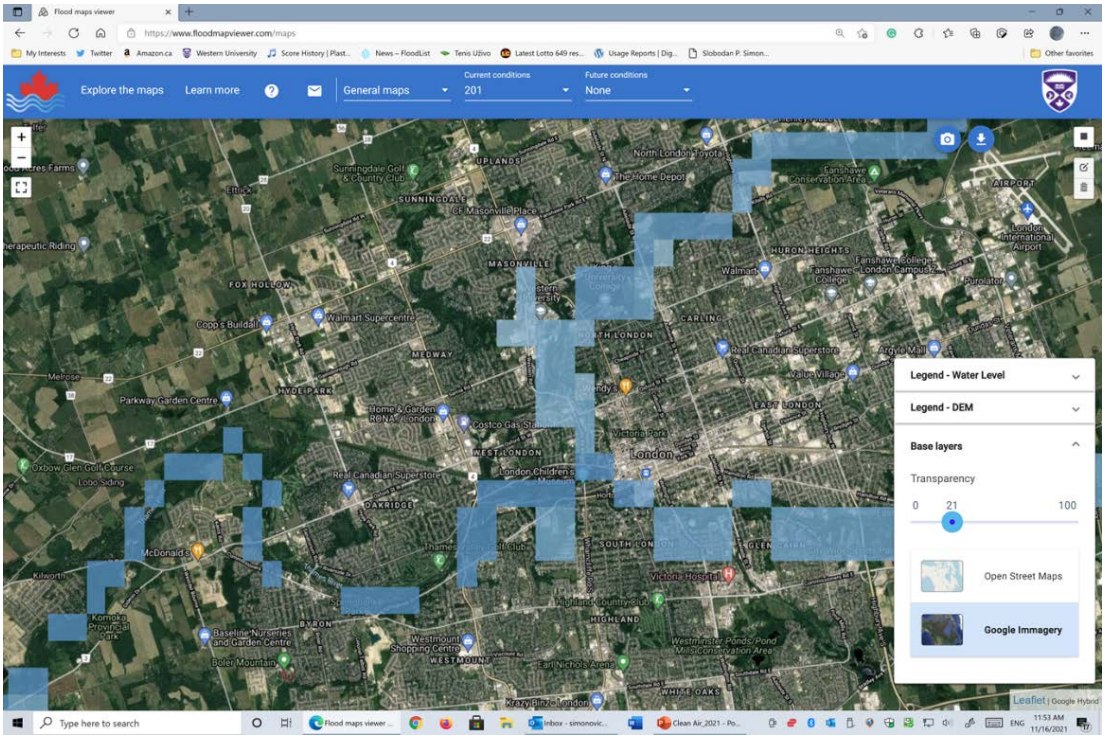

Figure 7. A representative illustration of the Flood Map Viewer (https://www.floodmapviewer.com/)

5. Conclusions

With the global rise of flood risk over several regions in the world, many countries are identifying the utility of floodplain mapping, as it provides both quantitative and qualitative information on impending risk. Despite many studies focusing over regional case-studies, the research on floodplain mapping has expanded to larger scales. This has been made possible with the ready availability of input datasets at high resolution, and at the same time state-of-the-art computational models responsible for replicating inundation dynamics. The present study explores the usability of publicly available datasets in characterizing flood hazard over Canada from the floodplain maps. It considers the NARR, a readily available reanalysis product, and other relevant datasets as major inputs to CaMa-Flood, a widely used robust flood modeling software to generate 100-yr and 200-yr floodplain maps. The simulated maps are compared and validated with the existing ones over a six different regions, based on which they are later used to quantify the degree of exposure of properties. The study demonstrates the worth of utilizing such datasets with a lesser degree of uncertainty in the flood model outputs. The floodplain maps derived from this study can be extended further to determine overall risk, by agglomerating vulnerability values. Such exhaustive information on flood risk may be considered as a precious cartographic product by the disaster management experts and city planners, which would further assist in selecting suitable flood control measures for an upgraded environmental development and management.

Author Contributions: Mohit Prakash Mohanty: Conceptualization, Methodology, Software, Data processing, Original draft preparation; Slobodan P. Simonovic: Supervision, Methodology, Results review, Reviewing and editing the manuscript.

Funding: The authors are grateful to the Natural Sciences and Engineering Research Council of Canada (NSERC) and the Institute for Catastrophic Loss Reduction (ICLR) for funding the research.

Data Availability Statement: The NARR runoff data is available for free download at https://psl.noaa.gov/. The CaMa-Flood model and its corresponding modules can be downloaded

from http://hydro.iis.u-tokyo.ac.jp/~yamadai/cama-flood/. Other relevant river and topographic related details are available on the same web address, and can be acquired from the developer upon reasonable request. The Canada-wide floodplain maps derived by utilizing NARR is available for visualization and free download at https://www.floodmapviewer.com/.

Acknowledgments: The authors thank Prof. Dai Yamazaki for providing CaMa-Flood version v4.01. The authors acknowledge SHARCNET (www.sharcnet.ca) for providing high super-computing facility for extensive model simulations. The exisiting floodplain maps over the six basins were collected from the respective river basin organisations. The authors are grateful to the Fraser Basin Council for providing 100-yr and 200-yr floodplain information over the Lower Fraser Basin. The authors acknowledge the Stats Canada for providing details on the property related information.

Conflicts of Interest: The authors declare no conflict of interest.

References

1. Alfieri, L., Bisselink, B., Dottori, F., Naumann, G., de Roo, A., Salamon, P., ... & Feyen, L. (2017). Global projections of river flood risk in a warmer world. Earth's Future, 5(2), 171-182.
2. Ashtine, M., Bello, R., & Higuchi, K. (2016). Assessment of wind energy potential over Ontario and Great Lakes using the NARR data: 1980–2012. Renewable and Sustainable Energy Reviews, 56, 272-282.
3. Bates, P. D., Horritt, M. S., & Fewtrell, T. J. (2010). A simple inertial formulation of the shallow water equations for efficient two-dimensional flood inundation modelling. Journal of Hydrology, 387(1-2), 33-45.
4. Bengtsson, L., Hagemann, S., & Hodges, K. I. (2004). Can climate trends be calculated from reanalysis data?. Journal of Geophysical Research: Atmospheres, 109(D11).
5. Bermúdez, M., Cea, L., Van Uytven, E., Willems, P., Farfán, J. F., & Puertas, J. (2020). A robust method to update local river inundation maps using global climate model output and weather typing based statistical downscaling. Water Resources Management, 34(14), 4345-4362.
6. Bernhofen, M. V., Whyman, C., Trigg, M. A., Sleigh, P. A., Smith, A. M., Sampson, C. C., ... & Winsemius, H. C. (2018). A first collective validation of global fluvial flood models for major floods in Nigeria and Mozambique. Environmental Research Letters, 13(10), 104007.
7. Blais, E.-L., Greshuk, J., Stadnyk, T., 2016. The 2011 flood event in the Assiniboine River Basin: causes, assessment and damages. Can. Water Resour. J./Revue canadienne des ressources hydriques 41 (1-2), 74–84. https://doi.org/10.1080/07011784.2015.1046139
8. Boulange, J., Hanasaki, N., Yamazaki, D., & Pokhrel, Y. (2021). Role of dams in reducing global flood exposure under climate change. Nature communications, 12(1), 1-7.
9. Chakraborty, L., Thistlethwaite, J., Minano, A., Henstra, D., & Scott, D. (2021). Leveraging Hazard, Exposure, and Social Vulnerability Data to Assess Flood Risk to Indigenous Communities in Canada. International Journal of Disaster Risk Science, 12(6), 821-838.
10. Compo, G. P., Whitaker, J. S., Sardeshmukh, P. D., Matsui, N., Allan, R. J., Yin, X., ... & Brönnimann, S. (2011). The twentieth century reanalysis project. Quarterly Journal of the Royal Meteorological Society, 137(654), 1-28.
11. Dottori, F., Szewczyk, W., Ciscar, J. C., Zhao, F., Alfieri, L., Hirabayashi, Y., ... & Feyen, L. (2018). Increased human and economic losses from river flooding with anthropogenic warming. Nature Climate Change, 8(9), 781-786.
12. Essou, G. R., Sabarly, F., Lucas-Picher, P., Brissette, F., & Poulin, A. (2016). Can precipitation and temperature from meteorological reanalyses be used for hydrological modeling?. Journal of Hydrometeorology, 17(7), 1929-1950.
13. Gaur, A., Gaur, A., & Simonovic, S. P. (2018). Future Changes in Flood Hazards across Canada under a Changing Climate. Water, 10(10), 1441.
14. Gaur, A., Gaur, A., Yamazaki, D., & Simonovic, S. P. (2019). Flooding related consequences of climate change on Canadian cities and flow regulation infrastructure. Water, 11(1), 63.
15. Gründemann, G. J., Werner, M., & Veldkamp, T. I. (2018). The potential of global reanalysis datasets in identifying flood events in Southern Africa. Hydrology and Earth System Sciences, 22(9), 4667-4683.
16. Hao, C., Yunus, A. P., Subramanian, S. S., & Avtar, R. (2021). Basin-wide flood depth and exposure mapping from SAR images and machine learning models. Journal of Environmental Management, 297, 113367.
17. Hawker, L., Rougier, J., Neal, J., Bates, P., Archer, L., & Yamazaki, D. (2018). Implications of simulating global digital elevation models for flood inundation studies. Water Resources Research, 54(10), 7910-7928.
18. Hunter, J. R., Woodworth, P. L., Wahl, T., & Nicholls, R. J. (2017). Using global tide gauge data to validate and improve the representation of extreme sea levels in flood impact studies. Global and Planetary Change, 156, 34-45.
19. Kim, S. J., Lee, M., Choi, W., & Rasmussen, P. F. (2008). Utilizing North American Regional Reanalysis for climate change impact assessment on water resources in central Canada. In Proceedings for the 13th World Water Congress, Montpellier, France (Vol. 14, pp. 1-4).
20. Kinoshita, Y., Tanoue, M., Watanabe, S., & Hirabayashi, Y. (2018). Quantifying the effect of autonomous adaptation to global river flood projections: application to future flood risk assessments. Environmental Research Letters, 13(1), 014006

21. Kirezci, E., Young, I. R., Ranasinghe, R., Muis, S., Nicholls, R. J., Lincke, D., & Hinkel, J. (2020). Projections of global-scale extreme sea levels and resulting episodic coastal flooding over the 21st Century. Scientific reports, 10(1), 1-12.
22. Lim, W. H., Yamazaki, D., Koirala, S., Hirabayashi, Y., Kanae, S., Dadson, S. J., ... & Sun, F. (2018). Long-term changes in global socioeconomic benefits of flood defenses and residual risk based on CMIP5 climate models. Earth's Future, 6(7), 938-954.
23. Liu, Y., Bates, P. D., Neal, J. C., & Yamazaki, D. (2021). Bare-Earth DEM Generation in Urban Areas for Flood Inundation Simulation Using Global Digital Elevation Models. Water Resources Research, 57(4), e2020WR028516.
24. Menéndez, P., Losada, I. J., Torres-Ortega, S., Narayan, S., & Beck, M. W. (2020). The global flood protection benefits of mangroves. Scientific reports, 10(1), 1-11
25. Mesinger, F., DiMego, G., Kalnay, E., Mitchell, K., Shafran, P. C., Ebisuzaki, W., ... & Shi, W. (2006). North American regional reanalysis. Bulletin of the American Meteorological Society, 87(3), 343-360.
26. Mohanty, M. P., & Simonovic, S. P. (2021). Changes in floodplain regimes over Canada due to climate change impacts: Observations from CMIP6 models. Science of The Total Environment, 792, 148323.
27. Mohanty, M. P., Vittal, H., Yadav, V., Ghosh, S., Rao, G. S., & Karmakar, S. (2020). A new bivariate risk classifier for flood management considering hazard and socio-economic dimensions. Journal of environmental management, 255, 109733.
28. Munich Re (2018). NatCatSERVICE database. Munich RE, Munich
29. NRCan (2018) Natural Resources Canada Federal Floodplain mapping Framework accessed on 10 March 2022.
30. Public Safety Canada (2017) Floods <https://www.publicsafety.gc.ca/cnt/mrgnc-mngmnt/ntrlhzrds/fld-en.aspx> accessed on 10 March 2022
31. Rannie, W. (2016). The 1997 flood event in the Red River basin: Causes, assessment and damages. Canadian Water Resources Journal/Revue canadienne des ressources hydriques, 41(1-2), 45-55.
32. Sampson, C. C., Smith, A. M., Bates, P. D., Neal, J. C., Alfieri, L., & Freer, J. E. (2015). A high-resolution global flood hazard model. Water resources research, 51(9), 7358-7381.
33. Senatore, A., Davolio, S., Furnari, L., & Mendicino, G. (2020). Reconstructing flood events in Mediterranean coastal areas using different reanalyses and high-resolution meteorological models. Journal of Hydrometeorology, 21(8), 1865-1887.
34. Simonovic, S. P. (1999). Decision support system for flood management in the Red River Basin. Canadian Water Resources Journal, 24(3), 203-223.
35. Smith, A., Bates, P. D., Wing, O., Sampson, C., Quinn, N., & Neal, J. (2019). New estimates of flood exposure in developing countries using high-resolution population data. Nature Communications, 10(1), 1-7.
36. Tarek, M., Brissette, F. P., & Arsenault, R. (2020). Evaluation of the ERA5 reanalysis as a potential reference dataset for hydrological modelling over North America. Hydrology and Earth System Sciences, 24(5), 2527-2544.
37. Tavares da Costa, R., Mazzoli, P., & Bagli, S. (2019). Limitations posed by Free DEMs in watershed studies: the case of river Tanaro in Italy. Frontiers in Earth Science, 7, 141.
38. Toosi, A. S., Doulabian, S., Tousi, E. G., Calbimonte, G. H., & Alaghmand, S. (2020). Large-scale flood hazard assessment under climate change: A case study. Ecological Engineering, 147, 105765.
39. UNISDR – The United Nations Office for Disaster Risk Reduction: The human cost of weather-related disasters 1995–2015, available at: https://www.unisdr.org/files/ 46796_cop21weatherdisastersreport2015.pdf (last access: 22 March 2022), 2015.
40. Vousdoukas, M. I., Mentaschi, L., Voukouvalas, E., Bianchi, A., Dottori, F., & Feyen, L. (2018). Climatic and socioeconomic controls of future coastal flood risk in Europe. Nature Climate Change, 8(9), 776-780.
41. Wang, N., Liu, W., Sun, F., Yao, Z., Wang, H., & Liu, W. (2020). Evaluating satellite-based and reanalysis precipitation datasets with gauge-observed data and hydrological modeling in the Xihe River Basin, China. Atmospheric Research, 234, 104746.
42. Ward, P. J., Jongman, B., Weiland, F. S., Bouwman, A., van Beek, R., Bierkens, M. F., ... & Winsemius, H. C. (2013). Assessing flood risk at the global scale: model setup, results, and sensitivity. Environmental Research Letters, 8(4), 044019.
43. Willner, S. N., Otto, C., & Levermann, A. (2018). Global economic response to river floods. Nature Climate Change, 8(7), 594-598.
44. Wing, O. E., Bates, P. D., Smith, A. M., Sampson, C. C., Johnson, K. A., Fargione, J., & Morefield, P. (2018). Estimates of present and future flood risk in the conterminous United States. Environmental Research Letters, 13(3), 034023.
45. Winsemius, H. C., Aerts, J. C., Van Beek, L. P., Bierkens, M. F., Bouwman, A., Jongman, B., ... & Ward, P. J. (2016). Global drivers of future river flood risk. Nature Climate Change, 6(4), 381-385
46. Winsemius, H. C., Van Beek, L. P. H., Jongman, B., Ward, P. J., & Bouwman, A. (2013). A framework for global river flood risk assessments. Hydrology and Earth System Sciences, 17(5), 1871-1892.
47. Yamazaki, D., Ikeshima, D., Tawatari, R., Yamaguchi, T., O'Loughlin, F., Neal, J. C., ... & Bates, P. D. (2017). A high-accuracy map of global terrain elevations. Geophysical Research Letters, 44(11), 5844-5853.
48. Yamazaki, D., Kanae, S., Kim, H., & Oki, T. (2011). A physically based description of floodplain inundation dynamics in a global river routing model. Water Resources Research, 47(4).
49. Yamazaki, D., Oki, T., & Kanae, S. (2009). Deriving a global river network map and its subgrid topographic characteristics from a fine-resolution flow direction map. Hydrology and Earth System Sciences, 13(11), 2241.
50. Yamazaki, D., O'Loughlin, F., Trigg, M. A., Miller, Z. F., Pavelsky, T. M., & Bates, P. D. (2014). Development of the global width database for large rivers. Water Resources Research, 50(4), 3467-3480.

 doi:10.20944/preprints202204.0086.v1

51. Yamazaki, D., Trigg, M. A., & Ikeshima, D. (2015). Development of a global~ 90 m water body map using multi-temporal Landsat images. Remote Sensing of Environment, 171, 337-351.